Effect of Pore-Network Connectivity on Multicomponent Adsorption of Large Molecules

S. Ismadji and S. K. Bhatia
Dept. of Chemical Engineering, The University of Queensland, St. Lucia, QLD 4072, Brisbane, Australia

The effect of pore-network connectivity on binary liquid-phase adsorption equilibria using the ideal adsorbed solution theory (IAST) was studied. The liquid-phase binary adsorption experiments used ethyl propionate, ethyl butyrate, and ethyl isovalerate as the adsorbates and commercial activated carbons Filtrasorb-400 and Norit ROW 0.8 as adsorbents. As the single-component isotherm, a modified Dubinin–Radushkevich equation was used. A comparison with experimental data shows that incorporating the connectivity of the pore network and considering percolation processes associated with different molecular sizes of the adsorptives in the mixture, as well as their different corresponding accessibility, can improve the prediction of binary adsorption equilibria using the IAST. Selectivity of adsorption for the larger molecule in binary systems increases with an increase in the pore-network coordination number, as well with an increase in the mean pore width and in the spread of the pore-size distribution.

Introduction

The purification and separation of the compounds from their mixtures can be carried out by several methods, such as distillation, extraction, and adsorption. The adsorption process itself has now become a standard unit operation in the chemical industry since it consumes low energy with separation efficiency comparable to other techniques.

The adsorption system usually involves more than one compound, and, therefore, the engineering design of the adsorption process requires information on multicomponent adsorption kinetics and equilibrium properties. As reliable experimental multicomponent adsorption isotherm data at various temperatures and concentrations are difficult and time-consuming to obtain, it is desirable to have a tool for predicting the multicomponent adsorption equilibrium based on single-component adsorption isotherms. For this purpose, various models and their modifications for describing multicomponent adsorption equilibria have been developed, such as extended Langmuir equation (Valenzuela and Myers, 1984; Yang, 1987), multisolute theory (Jossens et al., 1978), vacancy solution theory (Suwanayuen and Danner, 1980), Ideal adsorbed solution theory (IAST) (Myers and Prausnitz, 1965; Radke and Prausnitz, 1972), multispace adsorption model (Gusev et al., 1996), and other approaches (Jensen et al., 1997; Appel et al., 1998). Among these the IAST of Myers and Prausnitz (1965) is the most established and widely used method because of its generality and applicability to arbitrary single-component isotherms.

The Ideal adsorbed solution theory was developed based on the concept of creating the ideal multicomponent adsorbed phase by mixing pure adsorbed phases at a constant spreading pressure and temperature. The IAST is thermodynamically consistent and exact at the limit of zero pressure (Valenzuela and Myers, 1989). The IAST equation can be successfully applied with any type of single-component isotherm for a prediction of multicomponent adsorption equilibrium data (Costa et al., 1981; Richter et al., 1989). The successful application of the IAST for the prediction of the multicomponent isotherm depends on the correct choice of the single-component isotherm used (Richter et al., 1989; Hu and Do, 1995; Lavancy et al., 1996; Yun et al., 1996). Generally, the single-component isotherm used for the IAST prediction should give the best fit of the experimental data over the whole concentration range.

For heterogeneous adsorbents such as activated carbon, in many cases the IAST is inadequate to describe the experimental result because it does not account for the structural and chemical heterogeneity that is present in activated car-

Correspondence concerning this article should be addressed to S. K. Bhatia.

bon, and nonideality of the adsorbed mixture. In order to improve the IAST, the model has been extended using activity coefficients to develop real adsorbed solution theory (Talu and Zwiebel, 1986; Chen et al., 1990; Dunne and Myers, 1994), and heterogeneous surface models to describe the adsorbent (Moon and Tien, 1988; Valenzuela et al., 1988).

The structural heterogeneity of activated carbon is a result of the existence of micropores, mesopores, and macropores of different sizes and shapes, randomly connected in a pore network. In a pore network, some of the pores that are large enough to accommodate the probe molecules may be accessible only through smaller pores that only permit the passage of probe molecules having a smaller size. Therefore, only a part of the available pores is actually accessible to the probe molecules. The fraction of actually accessible pores is a function of the network topology, pore network connectivity, and the fraction of available pores (Seaton, 1991). The pore network connectivity is usually quantified as a mean coordination number Z. Different methods have been developed for determining the pore-network connectivity, and the most convenient method is the percolation theory interpretation of nitrogen sorption data (Neimark, 1991; Seaton, 1991). Another method based on molecular-size exclusion has been successfully applied for determining the pore-network connectivity for several porous solids (Lopez-Ramon et al., 1997; Lee and Tsay, 1998; Murray et al., 1998, 1999). In these studies, simple gas molecules, such as nitrogen, CH_4, CF_4, and SF_6, have been used. Most recently we (Ismadji and Bhatia, 2000, 2001a) have successfully utilized liquid-phase adsorption experimental data for determination of the pore-network connectivity of carbons. In these studies we used a large number of ester compounds, which have a more complex molecular structure, as probe molecules. In the adsorption process, especially involving large and complex probe molecules, the pore network connectivity is very important, and governs the transport and reaction properties of the pores. In this article we propose a method for incorporation of the pore-network connectivity along with the IAST to describe binary adsorption of large molecules from the liquid phase on activated carbons.

Model Development

Following the preceding discussion, percolation processes are important in the adsorption of large molecules, and not all the available pores are accessible to probe molecules. This feature provides additional complexities in the analysis of multicomponent adsorption based on single-component isotherms. In this section we first discuss the influence of percolation phenomena and accessibility on binary adsorption before presenting the single-component models used here. The latter have already been validated and presented in detail in our earlier articles (Ismadji and Bhatia, 2001a,b,c), and are described here only briefly for completeness.

Percolation processes in binary adsorption

The problem of pore-network accessibility, while straightforward for the single-component case, offers additional complexities in multicomponent adsorption of large molecules because of the differences in critical molecular sizes of the different components. To illustrate this we consider here the binary adsorption of two components. Component 1 has a critical molecular size, d_{c1}, smaller than the critical molecular size of component 2, d_{c2}. The adsorption behavior of the binary mixture is best described by considering four different groups of pores, as depicted in Figure 1. In the pore size between d_{c1} and d_{c2} ($d_{c1} < H < d_{c2}$), only pure component 1 is present (indicated as region I in Figure 1) since the pores in this region are not accessible to component 2. However, although the pores in this region are large enough to accommodate the probe molecules 1, some of these pores are connected through pores that are smaller in size than d_{c1}, and, therefore, are not accessible to these probe molecules. The amount of component 1 adsorbed in this region can be expressed as

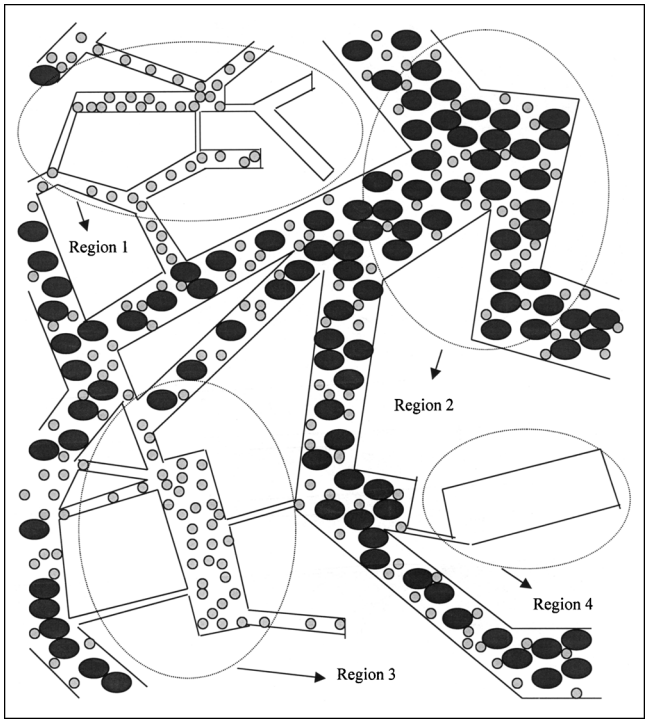

Figure 1. Binary adsorption process in micropore network.

$$q_{1a} = \frac{\Phi_{a1}}{\Phi_1} \int_{d_{c1}}^{d_{c2}} q_1^{\text{pure}}(H) f_n(H)\, dH \tag{1}$$

where $f_n(H)$ is the normalized pore volume distribution function, Φ_i is the fraction of available pores for component i

$$\Phi_i = \frac{\int_{d_{ci}}^{\infty} \frac{f_n(H)}{H} dH}{\int_0^{\infty} \frac{f_n(H)}{H} dH} \tag{2}$$

and Φ_{ai} is the fraction of the pores that are actually accessible to the probe molecules. A simple expression for Φ_{ai}, obtained by Zhang and Seaton (1996) from fits of simulation

results for cubic lattice, and generalized by Lopez-Ramon et al. (1997) to arbitrary and random lattices, is used in this work. The generalization is based on the concept of dimensional invariance, according to which the number of accessible pores per intersection is a universal function of the number of available pores (Sahimi, 1994). The resulting general expression has the form

$$\Phi_{ai} = 0, \qquad \Phi_i \le (1.494/Z) \tag{3}$$

$$\Phi_{ai} = \left[1.314(\Phi_i Z - 1.494)^{0.41} + 3.153(\Phi_i Z - 1.494) - 3.48(\Phi_i Z - 1.494)^2 + 1.433(\Phi_i Z - 1.494)^3\right]/Z, \quad (1.494/Z) < \Phi_i < (2.7/Z) \tag{4}$$

$$\Phi_{ai} = \Phi_i, \ \Phi_i \ge (2.7/Z) \tag{5}$$

where Z is the coordination number. The application of these expressions to the determination of Z from single-component adsorption data has recently been reported (Ismadji and Bhatia, 2000).

For the pores with sizes between d_{c2} and ∞, some of the pores are accessible to both compounds, so that a mixture of components 1 and 2 will be present within these latter pores (region 2). Furthermore, some of the pores larger than d_{c2} are connected by smaller pores that are smaller in size than d_{c2}. If the connecting pores have sizes between d_{c1} and d_{c2}, the component 1 can access these other larger pores (region 3). If the connecting pores have dimensions smaller than d_{c1}, the pores larger than d_{c2} will be inaccessible to both compounds (region 4). Therefore, the amount of component 1 adsorbed in this region can be written as

$$q_{1b} = \frac{\Phi_{a2}}{\Phi_2}\int_{d_{c2}}^{\infty} q_1^{\text{mix}}(H) f_n(H)\, dH + \left[\frac{\Phi_{a1}}{\Phi_1} - \frac{\Phi_{a2}}{\Phi_2}\right]\int_{d_{c2}}^{\infty} q_1^{\text{pure}}(H) f_n(H)\, dH \tag{6}$$

The total amount of component 1 adsorbed will be equal to $q_{1a} + q_{1b}$, leading to

$$q_{\text{tot1}}^{\text{mix}} = \frac{\Phi_{a1}}{\Phi_1}\int_{d_{c1}}^{\infty} q_1^{\text{pure}}(H) f_n(H)\, dH + \frac{\Phi_{a2}}{\Phi_2}\int_{d_{c2}}^{\infty}\left[q_1^{\text{mix}}(H) - q_1^{\text{pure}}(H)\right] f_n(H)\, dH \tag{7}$$

For component 2, the amount adsorbed is readily given by

$$q_{2,\text{tot}}^{\text{mix}} = \frac{\Phi_{a2}}{\Phi_2}\int_{d_{c2}}^{\infty} q_2^{\text{mix}}(H) f_n(H)\, dH \tag{8}$$

Equations 7 and 8 are valid for any single and binary component isotherm. We use a Dubinin–Radushkevich model modified to include bulk nonideality of the liquid phase and the repulsive potential in the micropores (Ismadji and Bhatia, 2001b) as the single-component isotherm. This is then used to determine a multicomponent isotherm based on the IAST. These isotherms are discussed in the following subsections.

Single-component isotherm

In predicting multicomponent adsorption equilibrium using the IAST method, the accuracy of the result depends on the correct choice of the single-component isotherm. An isotherm that fits the experimental data well over the whole concentration range is recommended for application, and here we use a modification of the Dubinin–Radushkevich equation as the single-component isotherm. Although details of the single-component model are available elsewhere (Ismadji and Bhatia, 2001b,c), for completeness we provide a brief description here.

The Dubinin–Radushkevich (DR) equation has a uniform general form that is useful for most adsorbates and follows the expression

$$q_i = Q_{\text{max},i}\exp\left[-\left(\frac{A_i}{\beta_i E_o(H)}\right)^2\right] \tag{9}$$

where q_i and $Q_{\text{max},i}$ are the amount adsorbed and the maximum capacity for component i in the pore, respectively. Furthermore, β_i is an affinity coefficient and $E_o(H)$ is characteristic energy. The maximum capacity, $Q_{\text{max},i}$, has the temperature dependence

$$Q_{\text{max},i} = Q_{\text{max},i}^0 \exp\left[\delta_i(T_o - T)\right] \tag{10}$$

where $Q_{\text{max},i}^o$ is the actual maximum capacity at reference temperature T_o (taken here as 303.15 K), and δ_i is a constant parameter representing the temperature coefficient of expansion of the adsorbate. The nonideality of the bulk liquid phase is crucially important, as described in our previous papers (Ismadji and Bhatia, 2000, 2001b,c). To account for the bulk liquid phase nonideality, the adsorption potential is represented in terms of activities:

$$A_i = RT\ln\left(\frac{a_{s,i}}{a_i}\right) \tag{11}$$

in which the activity coefficient for each species is estimated through the UNIFAC group-contribution model (Sandler, 1999). This is a departure from the usual relations for A_i in terms of concentrations or pressures, which ignore nonideality.

The usual form of the characteristic energy in the DR equation, $\beta_i E_o(H) = \beta_i k/H$, does not include the repulsive interaction that is important at molecular scales, and can only approximate attractive interactions with the pore walls. This deficiency has also been observed in one of our previous articles (Ismadji and Bhatia, 2001b), and to alleviate this shortcoming, here we express the characteristic energy term, $\beta_i E_o(H)$, in terms of the fluid–solid interaction energy

$$\beta_i E_o(H) = \tau_i\left[\Theta_{\text{min}}(H) - \Theta_{\text{min}}^{\infty}\right] \tag{12}$$

where τ_i is a constant, $\Theta_{\text{min}}(H)$ and $\Theta_{\text{min}}^{\infty}$ are the minimum potential in a micropore of width H and the minimum potential on a flat surface, respectively. To describe the adsorption potential between the fluid molecules and the micropore

walls, we use the 10-4-3 potential model of Steele (1973) for a semi-infinite carbon slab that has the form

$$\Omega_{CA}(z) = 2\pi\rho_C \epsilon_{CA} \sigma_{CA}^2 \Delta \left[\frac{2}{5}\left(\frac{\sigma_{CA}}{z}\right)^{10} - \left(\frac{\sigma_{CA}}{z}\right)^4 - \left(\frac{\sigma_{CA}^4}{3\Delta(0.61\Delta + z)^3}\right)\right] \quad (13)$$

where z is the distance from the centers of the surface atoms of a carbon wall, ρ_C (114 nm^{-3}) is the carbon density, and Δ (= 0.335 nm) is the interlayer spacing. The Lennard-Jones (LJ) parameters for the adsorbate–adsorbent interaction, ϵ_{CA} and σ_{CA} were calculated using the Berthelot rules

$$\epsilon_{CA} = \sqrt{\epsilon_{CC}\epsilon_{AA}}, \qquad \sigma_{CA} = \frac{\sigma_{CC} + \sigma_{AA}}{2} \quad (14)$$

Here σ_{ii} is the molecular-size parameter, and ϵ_{ii} is the potential well depth for the adsorptive LJ potential. For the carbon atoms, the LJ molecular-size parameter was taken as 0.3354 nm, and the potential well depth parameter ϵ_{CC}/k = 28.0 K (Steele, 1973). For carbons having slitlike pores between walls that are infinite in both lateral directions, the pore potential is the total contribution from each side

$$\Theta(H', z) = \Omega_{CA}(z) + \Omega_{CA}(H' - z) \quad (15)$$

where H' is the center-to-center distance between carbon atoms on opposing pore walls, related to the physical pore width H by

$$H' = H + 0.3354 \quad (16)$$

The minimum values of the adsorption potential in the micropore and on the flat surface are achieved at a distance $z_{\min}$ and $z_{\min}^{\infty}$, respectively, and can be written as

$$\Theta_{\min}(H) = \Theta(H', z_{\min}) + \Omega_{CA}(z_{\min}) + \Omega_{CA}(H' - z_{\min}) \quad (17)$$

and

$$\Theta_{\min}^{\infty} = \Theta^{\infty}(z_{\min}^{\infty}) = \Omega_{CA}(z_{\min}^{\infty}) \quad (18)$$

which combine with Eq. 12 to provide

$$\beta_i E_o(H) = \tau_i\left[\Theta(H', z_{\min}) - \Theta^{\infty}(z_{\min}^{\infty})\right] \quad (19)$$

The final form of the modified DR equation is now expressed as

$$q_i = Q_{\max,i}^o \exp\left[\delta_i(T_o - T)\right] \exp\left[-\left(\frac{RT\ln(a_{s,i}/a_i)}{\tau_i\left[\Theta(H', z_{\min}) - \Theta^{\infty}(z_{\min}^{\infty})\right]}\right)^2\right] \quad (20)$$

Equation 20 also can be written in the generalized adsorption isotherm form

$$q_i = Q_{\max,i}^o \int_{d_{c,i}}^{\infty} \exp\left[\delta_i(T_o - T)\right] \exp\left[-\left(\frac{RT\ln(a_{s,i}/a_i)}{\tau_i\left[\Theta(H', z_{\min}) - \Theta^{\infty}(z_{\min}^{\infty})\right]}\right)^2\right] f_n(H)\, dH \quad (21)$$

Multicomponent formulation

In developing a multicomponent isotherm model, based on the single-component isotherm just discussed, the ideal adsorbed solution theory of Myers and Prausnitz (1965) has been utilized. The IAST theory was developed based on the assumption that the adsorbed phase can be treated as an ideal solution of the adsorbed components, and its application usually considers the ideal bulk phase as well. For a nonideal bulk fluid, the Gibbs adsorption equation may be written as

$$V d\phi = q_i^{\text{pure}} d\mu_i^a = q_i^{\text{pure}} RT d\ln(a_i) \quad (22)$$

where μ_i is the chemical potential of solute i, and ϕ is a three-dimensional spreading pressure. Integration of Eq. 22 leads to

$$\Pi_i = \frac{\phi V}{RT} = \int_0^{a_i^o} \frac{q_i^{\text{pure}}}{a_i} da_i = \Pi = \text{constant} \quad (23)$$

For the multicomponent adsorbate, if the solute in the bulk solution is in equilibrium with the adsorbed species

$$d\mu_i^b = d\mu_i^a \qquad \text{or} \qquad RT d\ln(a_i) = RT d\ln(x_i) \quad (24)$$

where μ_i^b and μ_i^a are the chemical potential of species i in the bulk solution and in adsorbed phase, respectively. Equation 24 can be integrated with the condition $x_i = 1$ for $a_i = a_i^o$ to yield

$$a_i = a_i^o x_i \quad (25)$$

The adsorbed-phase compositions must satisfy the requirement

$$\sum_{i=1}^{N} x_i = 1 \quad (26)$$

The total amount adsorbed, q_T, at a given temperature and spreading pressure is a function only of the adsorbed-phase compositions, x_i, and the pure component amounts adsorbed, q_i, at a fixed spreading pressure

$$q_T = \left[\sum_{i=1}^{N} \frac{x_i}{q_i^o}\right]^{-1} \quad (27)$$

where $q_i^o = q_i^{\text{pure}}$ (a_i^o), that is, q_i^{pure} evaluated at $a_i = a_i^o$. The amount adsorbed for each species now can be determined by

$$q_i^{mix} = x_i q_T \quad (28)$$

For the IAST application, Eq. 20 is modified to

$$q_i^{\text{pure}} = Q^o_{\max,i}\frac{\Phi_i}{\Phi_{a,i}}\exp\left[\delta_i(T_o - T)\right] \exp\left[-\left(\frac{RT\ln(a_{s,i}/a_i)}{\tau\left[\Theta(H', z_{\min}) - \Theta^{\infty}(z^{\infty}_{\min})\right]}\right)\right] \quad (29)$$

as the fitted capacity, $Q^o_{\max,i}$ in Eq. 20 includes the network accessibility factor. To separate the latter, we multiply by the factor $\Phi_i/\Phi_{a,i}$. Thus, q_i^{pure} represents the isotherm for pure component i, if all available pores (that is pores larger than d_{ci}) are accessible. Substitution of Eq. 29 into Eq. 23 leads to the analytical result

$$\Pi_i = \frac{B}{RT}Q^o_{\max,i}\frac{\Phi_i}{\Phi_{a,i}} \exp\left[\delta_i(T_o - T)\right]\frac{\sqrt{\pi}}{2}\left[1 - erf\left[\frac{RT}{B}\ln\left(\frac{a_{s,i}}{a_i^o}\right)\right]\right] \quad (30)$$

which was used in conjunction with Eqs. 25–28, with $B = [\tau(H', z_{\min}) - \Theta^{\infty}(z^{\infty}_{\min})]$, to obtain the multicomponent isotherms for each component in a pore of actual width H $(= H' - 0.3354)$.

Experimental Section

Materials

The adsorbents used in this study are commercial activated carbons Filtrasorb 400 and Norit ROW 0.8. Prior to use, the carbons were washed several times using reverse-osmosis water in order to remove fine particles, and subsequently dried and degassed under nitrogen flowing at 523.15 K for 24 h. The activated carbons were characterized using argon adsorption. The measurement of the argon adsorption isotherm was carried out at 87.15 K using an automatic Micromeritics ASAP-2010 volumetric sorption analyzer. The structural characteristics of the activated carbons are shown in Table 1. The pore-size distributions of the activated carbons were determined using the Micromeritics nonlocal density functional theory (DFT) software, with minimum regularization.

Table 1. Structural Characteristics of Activated Carbons

Sorption Characteristics	Filtrasorb 400	Norit ROW 0.8
BET surface area, m^2/g	877.82	849.39
Micropore surface area, m^2/g	761.80	718.00
Micropore volume, cm^3/g	0.343	0.314
Total pore volume, cm^3/g	0.468	0.443

Three different flavor compounds: ethyl propionate, ethyl butyrate, and ethyl isovalerate, were used as the adsorbates in this study. These compounds were obtained as an analytical grade with a purity of about 98–99% from Sigma Aldric Pty. Ltd. (NSW, Australia), and used without any further purification.

Adsorption experiments

The adsorption isotherm for binary systems of ethyl propionate, ethyl butyrate, and ethyl isovalerate from aqueous solution on Filtrasorb 400 and Norit ROW 0.8 were obtained isothermally at three different temperatures, 303.15 K, 308.15 K, and 313.15 K. Fixed amounts (0.1 dm^3) of the binary solutions having desired solute concentrations (0.1–1.2 kg/m^3) were placed in a series of 0.1-dm^3 glass-stoppered flasks. The

Table 2. Fitted Parameters of the Single-Component Isotherm Using Bimodal Gamma Function as Pore Size Distribution

	Parameter							
Adsorptive	$Q^o_{\max}$, kg/kg	$\delta_i \times 10^{-3}$, K^{-1}	τ_i	w_1	α_1	w_2	α_2	b_1
			Filtrasorb 400					
Ethyl propionate	0.36514	2.143	0.384					
Ethyl butyrate	0.40612	3.102	0.316	36.81	16.73	3.18	3.05	0.318
Ethyl isovalerate	0.35216	3.541	0.369					
			Norit ROW 0.8					
Ethyl propionate	0.35261	2.412	0.404					
Ethyl butyrate	0.39318	3.359	0.319	65.87	30.44	2.34	2.16	0.348
Ethyl isovalerate	0.34027	3.714	0.369					

Table 3. Fitted Parameters of the Single-Component Isotherm Using DFT-Based Pore-Size Distribution

Adsorptive	$Q^o_{\max}$, kg/m^3	$\delta_i \times 10^{-3}$ K^{-1}	τ_i
	Filtrasorb 400		
Ethyl propionate	723.47	2.364	0.425
Ethyl butyrate	784.16	2.408	0.366
Ethyl isovalerate	666.05	3.357	0.443
	Norit ROW 0.8		
Ethyl propionate	765.38	2.415	0.426
Ethyl butyrate	860.54	2.914	0.355
Ethyl isovalerate	738.50	3.322	0.409

bottles were then placed in a controlled temperature shaker water bath. After the temperature of the solutions reached the desired temperature, known amounts of activated carbon were added to the binary solutions. Equilibrium was achieved within 24 to 48 h, with the initial and equilibrium concentrations of the binary solutions analyzed by means of a Shimadzu gas chromatograph (GC-17A) provided with a flame ionization detector, and the amount adsorbed obtained by the material balance.

Results and Discussion

Prediction of binary isotherms

Prior to predicting binary isotherms the fitted parameters for single-component adsorption of ethyl propionate, ethyl butyrate, and ethyl isovalerate were obtained by two different methods (Ismadji and Bhatia, 2001a). The first method used a normalized bimodal gamma function as the pore-size distribution (PSD) to fit the data, and the second used the known DFT-based PSD (obtained using argon adsorption) for fitting the data. The normalized bimodal gamma function has the following form

$$f_n(H) = b_1 \frac{w_1^{\alpha_1+1} H^{\alpha_1} e^{-w_1 H}}{\Gamma(\alpha_1+1)} + (1-b_1) \frac{w_2^{\alpha_2+1} H^{\alpha_2} e^{-w_2 H}}{\Gamma(\alpha_2+1)} \quad (31)$$

where $\Gamma(\alpha_i+1)$ is the gamma function, while w_i and α_i are pore structural parameters, and b_1 is the fraction of the pore volume associated with the first peak. Tables 2 and 3 summarize the fitted parameters obtained from bimodal gamma function fitting and DFT-based PSD fitting, respectively. Details of the fitting procedures are available elsewhere (Ismadji and Bhatia, 2001a). From the fitted capacities, the mean coordination numbers, Z, of the adsorbents used were estimated as 3.22 for Filtrasorb 400 and 3.95 for Norit ROW 0.8, based on fits using the DFT-based PSD. Using the bimodal gamma distribution fitting, the coordination number was obtained as 4.03 for Filtrasorb 400 and 4.84 for Norit ROW 0.8. These values are marginally different from those reported earlier (Ismadji and Bhatia, 2001a) as a result of improved fitting of the single-component isotherm. The normalized bimodal gamma function can be related to the volumetric PSD $f(H)$ following

$$f_n(H) = \frac{f(H)}{V_T} \quad (32)$$

where V_T is the total specific pore volume of the adsorbent. Figure 2 depicts the PSD of Filtrasorb-400 and ROW 0.8.

As discussed earlier, binary adsorption equilibrium data have been obtained for the adsorption of ethyl propionate, ethyl butyrate, and ethyl isovalerate on activated carbons Filtrasorb 400 and Norit ROW 0.8. The effect of the pore-network connectivity was taken into account in the prediction of the binary adsorption isotherms using the IAST method, following the model presented here. The agreement between the binary component adsorption experimental data and that predicted by our proposed model is shown in Figures 3–8. These figures show individual isotherms for adsorption of a given compound in the presence of various starting concentrations of the other compound on activated carbon F 400 and Norit ROW 0.8. In these figures, the experimental data are indicated by symbols, while the solid lines represent the predicted values based on single-component isotherm fits using the DFT-based PSD. The insets in Figures 3–8 indicate the experimental data and predicted values using the fitted bimodal gamma function as the pore-size distribution. In general, the model can represent the experimental data fairly well with both PSDs, as seen in Figures 3–8. The small difference between the binary isotherms predicted by the model with bimodal gamma function PSD and those using the DFT-based distribution is most likely due to the constraint of the gamma function bimodal form.

The mutual interference of ethyl propionate, ethyl butyrate, and ethyl isovalerate is very different, as indicated by the data in Figures 3–8. Ethyl propionate and ethyl butyrate

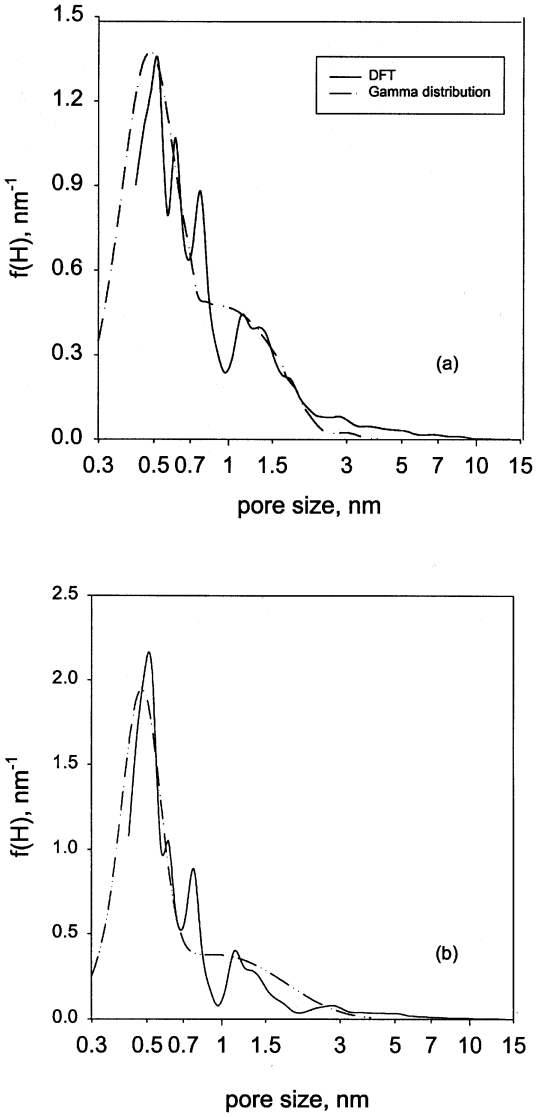

Figure 2. DFT-based and gamma function-based pore-size distribution of (a) Filtrasorb 400, and (b) Norit ROW 0.8.

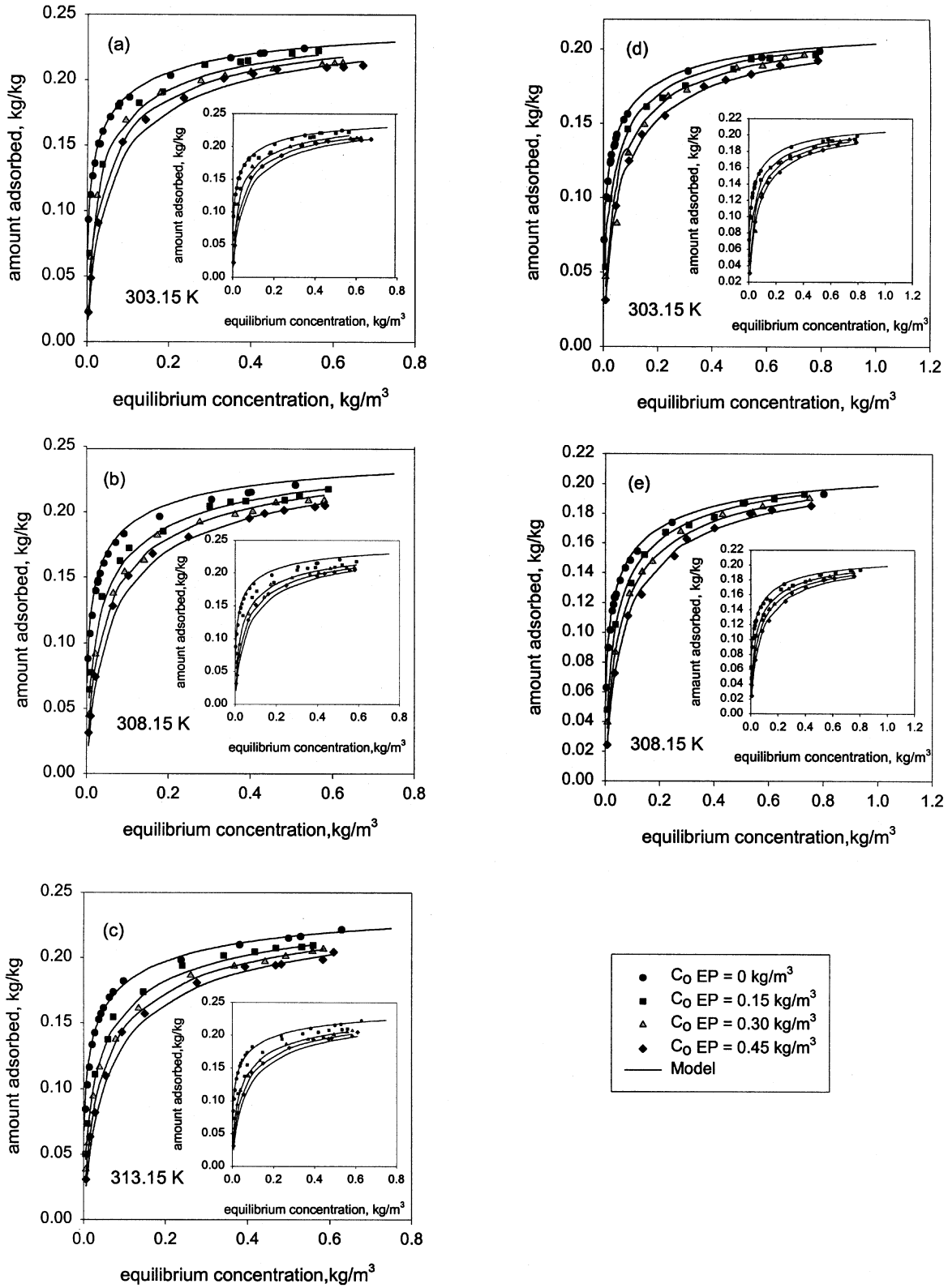

Figure 3. Adsorption isotherms of ethyl isovalerate in the presence of ethyl propionate, and model results with DFT-based distribution.

Insets are the model results with gamma-function distribution. (a)–(c) Filtrasorb 400, and (d)–(e) Norit ROW 0.8.

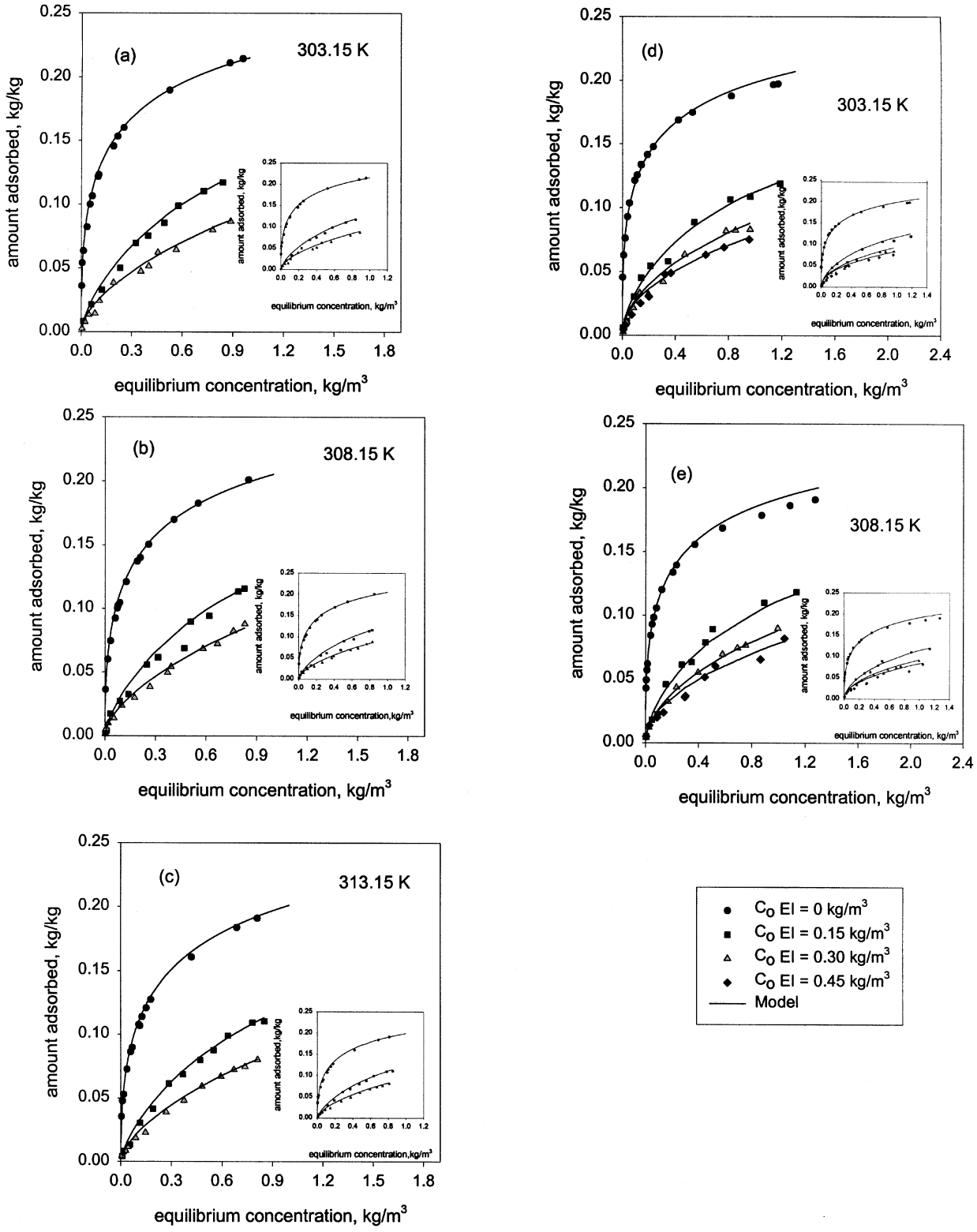

Figure 4. Adsorption isotherms of ethyl propionate in the presence of ethyl isovalerate, and model results with DFT-based distribution.

Insets are the model results with gamma-function distribution. (a)–(c) Filtrasorb 400, and (d)–(e) Norit ROW 0.8.

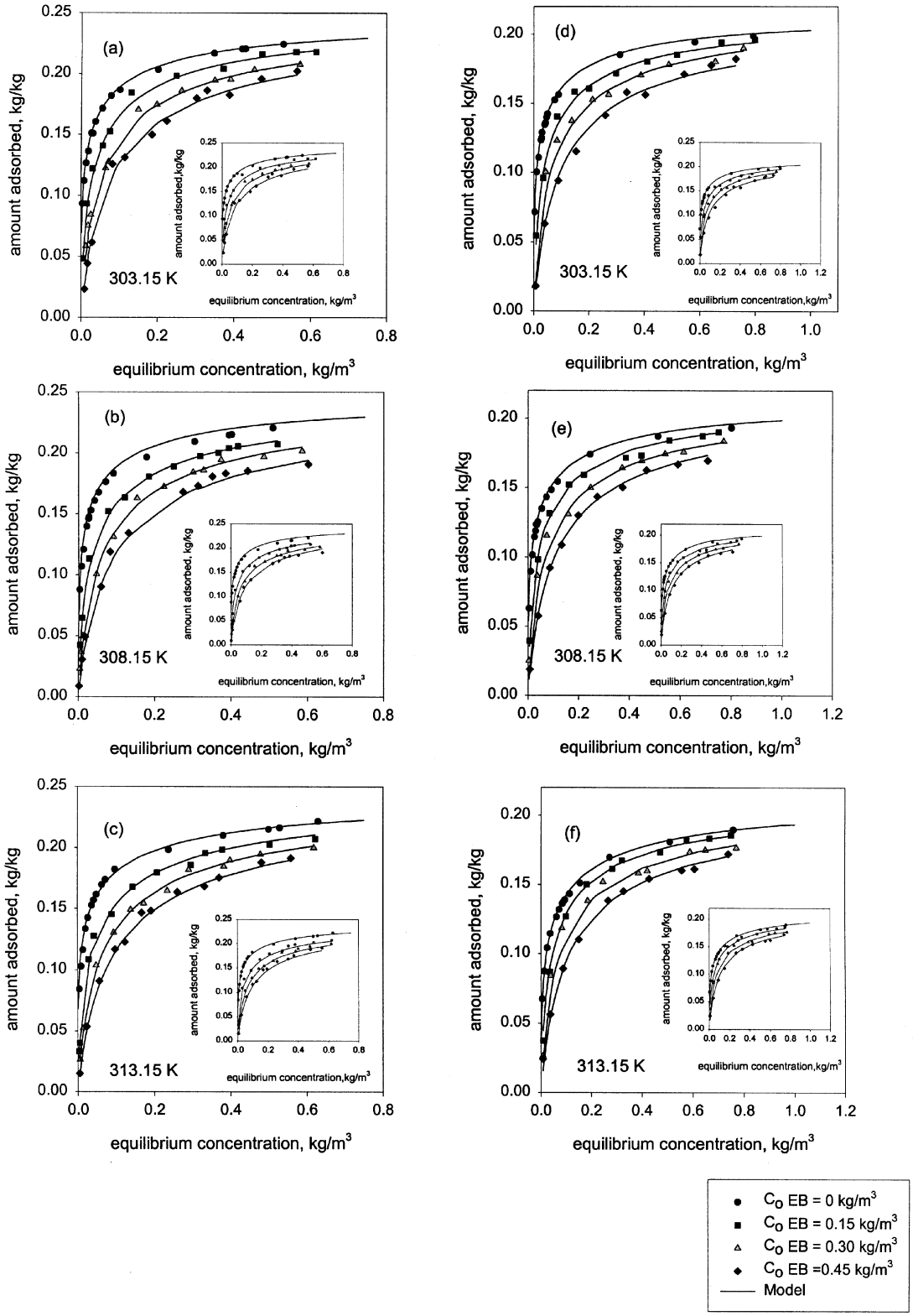

Figure 5. Adsorption isotherms of ethyl isovalerate in the presence of ethyl butyrate, and model results with DFT-based distribution.

Insets are the model results with gamma-function distribution. (a)–(c) Filtrasorb 400, and (d)–(f) Norit ROW 0.8.

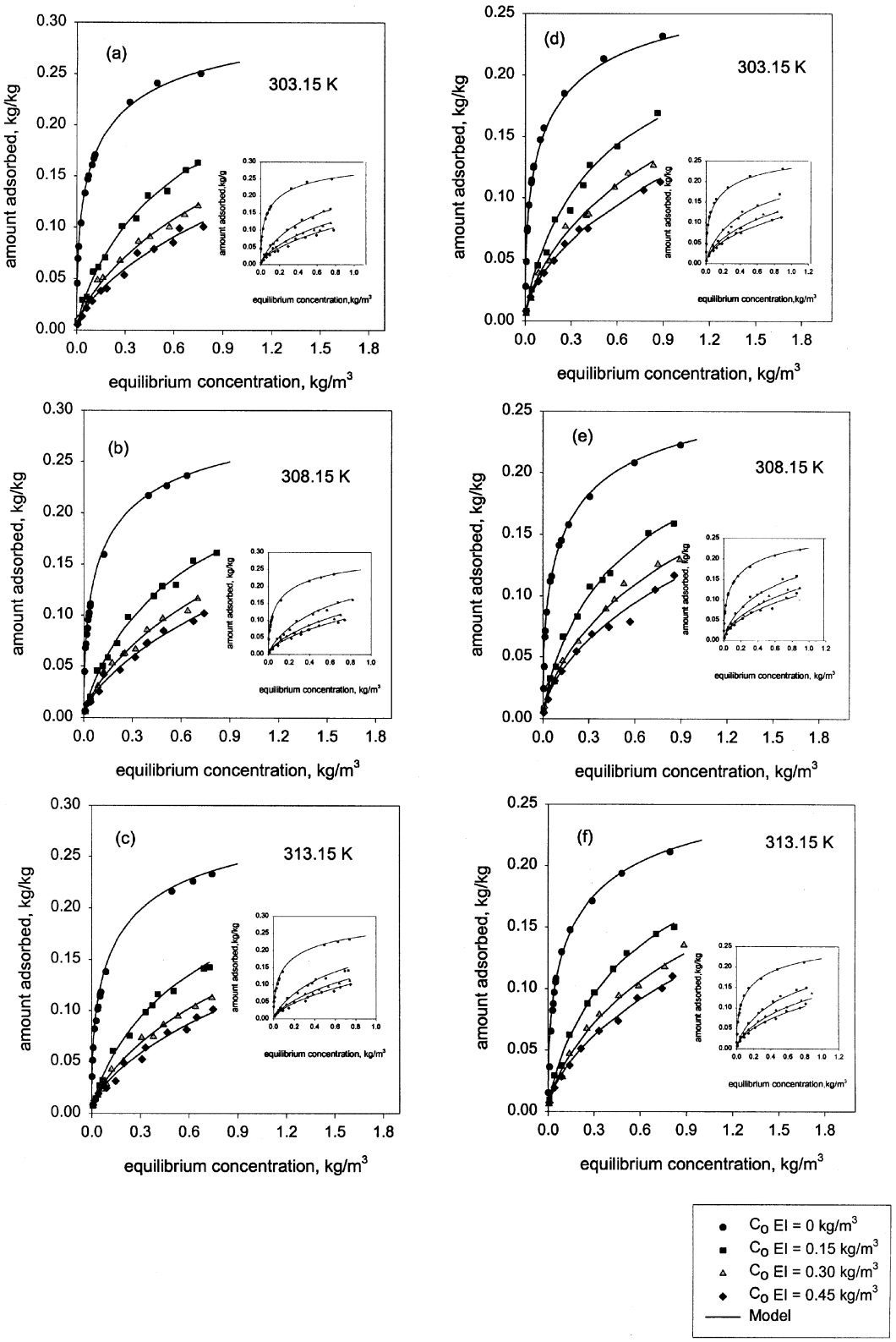

Figure 6. Adsorption isotherms of ethyl butyrate in the presence of ethyl isovalerate, and model results with DFT-based distribution.

Insets are the model results with gamma-function distribution. (a)–(c) Filtrasorb 400, and (d)–(f) Norit ROW 0.8.

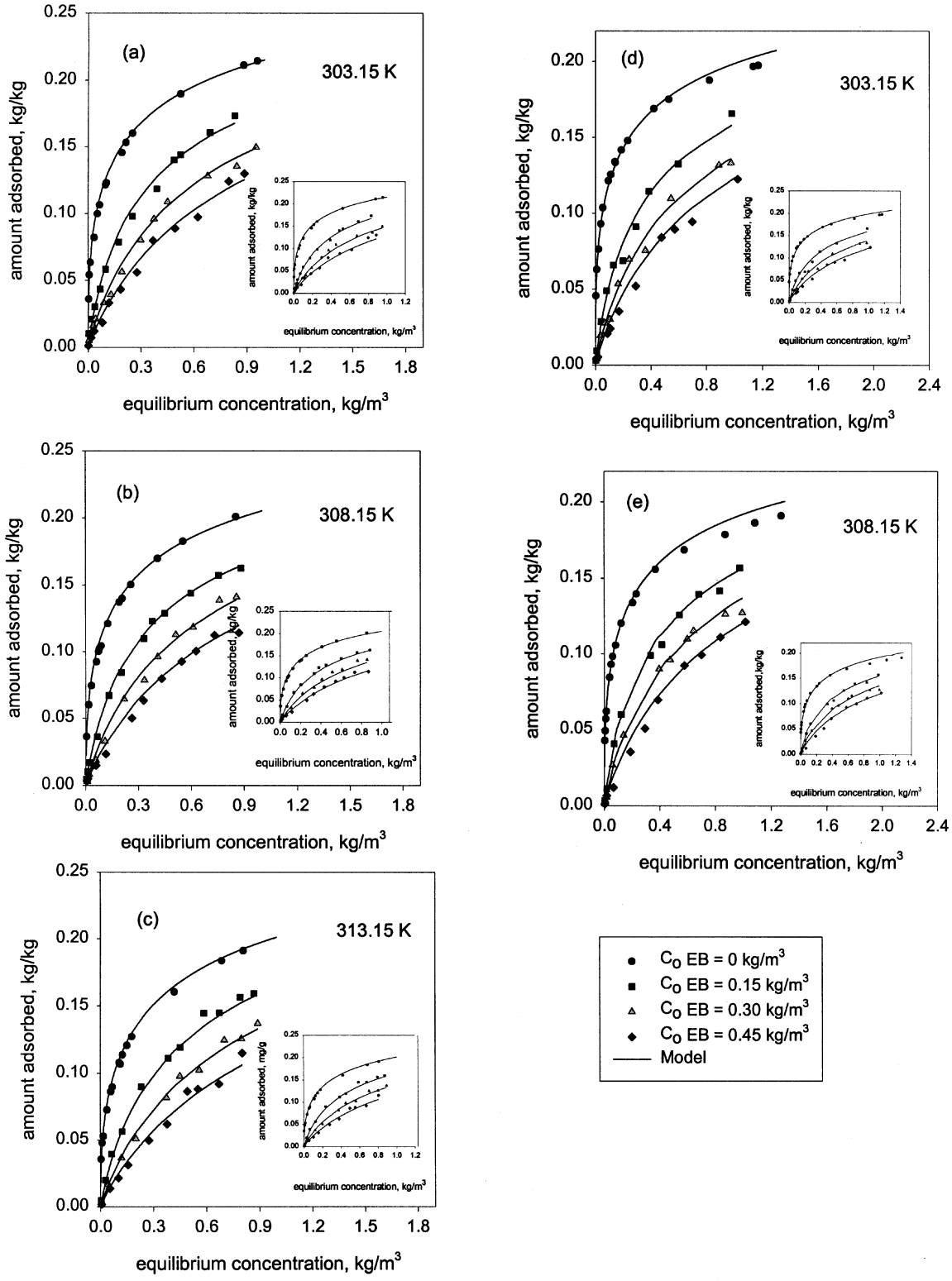

Figure 7. Adsorption isotherms of ethyl propionate in the presence of ethyl butyrate, and model results with DFT-based distribution.

Insets are the model results with gamma-function distribution. (a)–(c) Filtrasorb 400, and (d)–(e) Norit ROW 0.8.

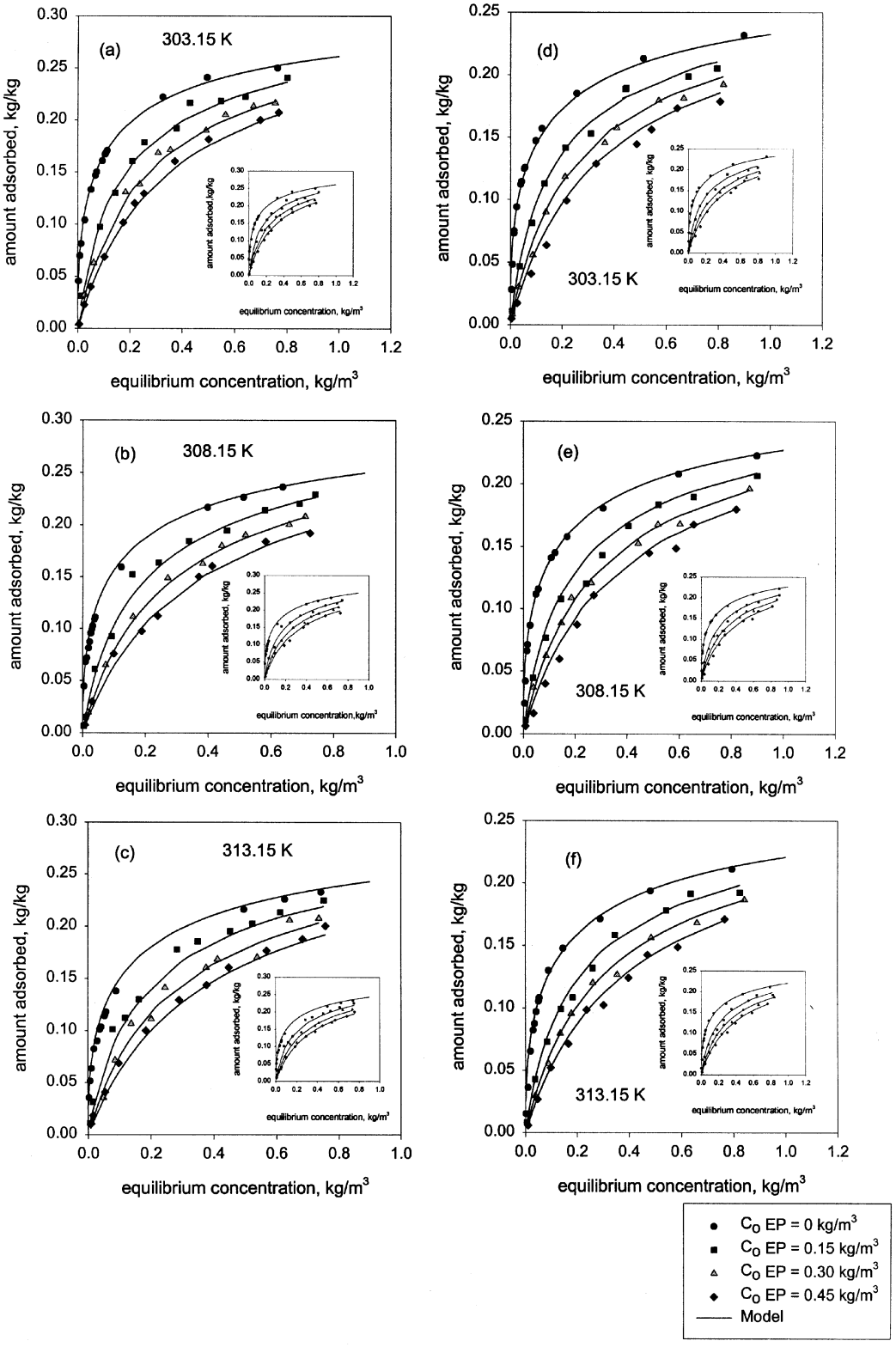

Figure 8. Adsorption isotherms of ethyl butyrate in the presence of ethyl propionate, and model results with DFT-based distribution.

Insets are the model results with gamma-function distribution. (a)–(c) Filtrasorb 400, and (d)–(f) Norit ROW 0.8.

compete relatively weakly for the adsorption sites compared to ethyl isovalerate. This is evident in Figs. 3 and 5, where ethyl isovalerate adsorption is only moderately affected by the presence of the other two compounds, while the amount of ethyl propionate and ethyl butyrate adsorbed sharply decreases in the presence of ethyl isovalerate (Figures 4 and 6). The ethyl butyrate also gives stronger competition than ethyl propionate, as seen in Figures 7 and 8. This behavior is readily rationalized, since in adsorption of organic compounds in the liquid phase, the critical molecular size of the compound plays a strong role. Qualitatively, the interaction forces between the adsorbate molecules and the pore walls become stronger as the critical molecular size of the compound increases. For the three esters used in this study, the critical molecular sizes of the esters follows the order, ethyl isovalerate > ethyl butyrate > ethyl propionate (Ismadji and Bhatia, 2001a). The critical molecular sizes of the esters used in this study are 0.577 nm for ethyl isovalerate, 0.539 nm for ethyl butyrate, and 0.511 nm for ethyl propionate. Since the ethyl isovalerate has the highest critical molecular size, the interaction force of this molecule is stronger compared with ethyl butyrate and ethyl propionate, and it tends to compete much more strongly.

Importance of pore-network connectivity

In order to test the importance of the incorporation of the pore-network connectivity concept, we also applied the ideal adsorbed solution theory, without considering the connectivity of the pore network, to describe the binary adsorption experimental data of the ethyl butyrate–ethyl isovalerate system. For the purposes of this test the single-component isotherms and fits using the DFT-based PSD were used. The binary predictions were obtained using the IAST with Eq. 20 as the pure-component isotherm, so that the accessibility factor was not separated out. The overall isotherm for each component then follows

$$q_{i,\text{app}} = q_{i,\text{tot}}^{\text{mix}} = \int_{d_{ci}}^{\infty} q_i^{\text{mix}}(H) f_n(H)\, dH \tag{33}$$

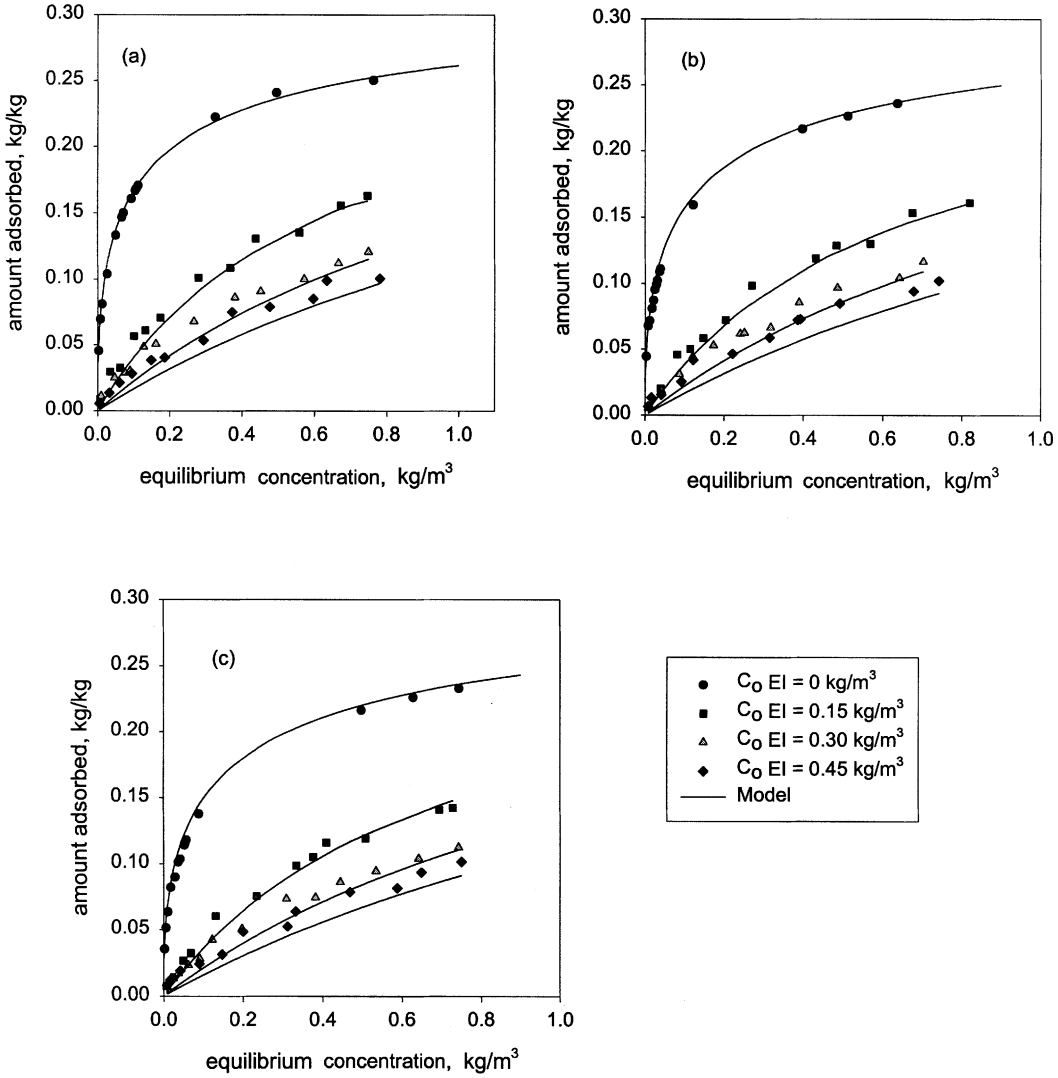

Figure 9. Adsorption isotherms of ethyl butyrate in the presence of ethyl isovalerate on Filtrasorb–400 activated carbon, and predicted value neglecting percolation effects: (a) 303.15 K, (b) 308.15 K, and (c) 313.15 K.

Figure 9 depicts the binary adsorption experimental data of the ethyl butyrate–ethyl isovalerate system and the predicted values obtained from the preceding method. From this figure, it is evident that the predicted values obtained by this method are somewhat lower than the actual adsorbed amounts obtained from experiments. This is due to the fact that actually pure-component adsorption of ethyl butyrate occurs in those pores not accessible to ethyl isovalerate, an effect that enhances ethyl butyrate adsorption. As expected the error is higher with the increase in concentration of the larger component (ethyl isovalerate). On the other hand, when the percolation effect and accessibility factor were appropriately considered the predictions were far more accurate, as seen in Figures 3–8. Quantitatively, for the data in Figure 9, it was found that the prediction error increased from about 2% to 5% percent (when connectivity is considered) to about 10% to 80% when connectivity effects are ignored. In the latter case, the error is particularly high, and as high as 80%, at low concentrations. Since the experimental error in determining concentration is within 10%, this evidence strongly indicates that the connectivity of the pore network has significant influence and must be considered in the calculation of multicomponent isotherms using the IAST method.

Effect of pore-structure parameters

Figures 10–13 depict the effect of pore-structural parameters on the selectivity and fraction error if the percolation effect is neglected, in binary adsorption of ethyl propionate–ethyl isovalerate mixtures using parameters for Filtrasorb 400 activated carbon. Bulk concentrations of ethyl propionate and ethyl isovalerate of 0.398 kg/m^3 and 0.07189 kg/m^3, respectively, were assumed. As the pore-size distribution we chose an arbitrary single gamma function distribution of the form

$$f_n(H) = \frac{w^{\alpha+1} H^{\alpha} e^{-wH}}{\Gamma(\alpha+1)} \tag{34}$$

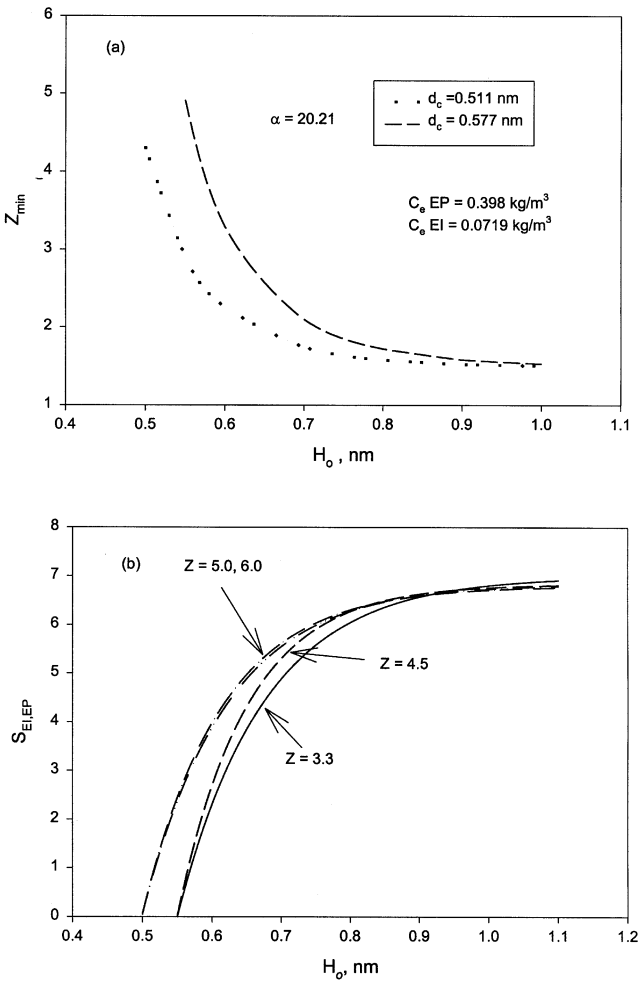

Figure 10. Effect of mean pore width on (a) minimum coordination number and (b) selectivity on adsorption of ethyl propionate/ethyl isovalerate system on Filtrasorb 400 activated carbon.

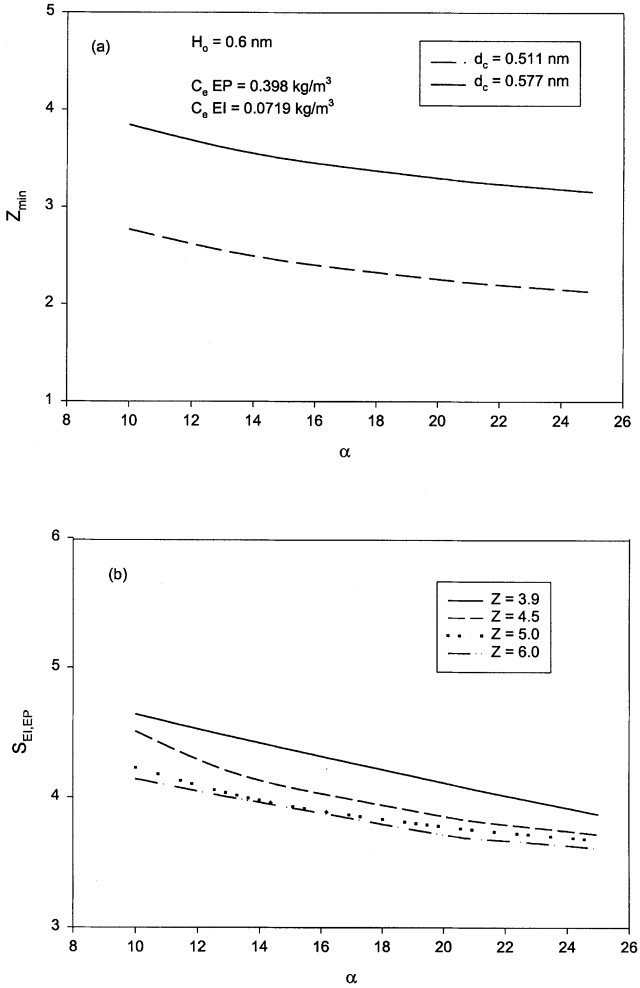

Figure 11. Effect of gamma-function parameter α on (a) minimum coordination number and (b) selectivity on adsorption of ethyl propionate/ethyl isovalerate system on Filtrasorb 400 activated carbon.

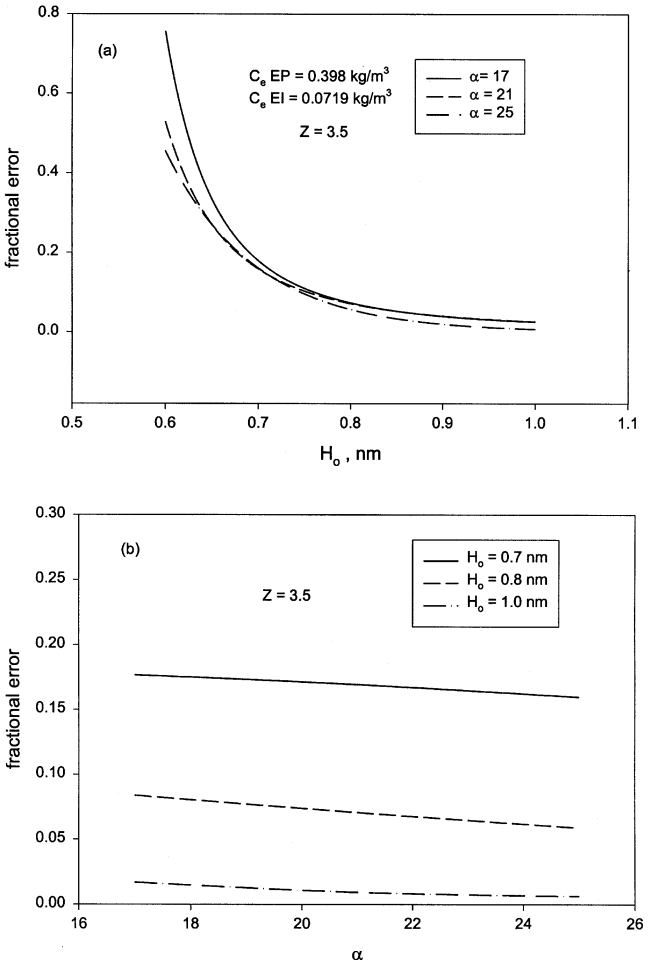

Figure 12. Effect of the gamma-function parameter on the fraction of error of the amount of ethyl propionate adsorbed if percolation effects are neglected.

Effect of (a) mean pore width and (b) parameter α.

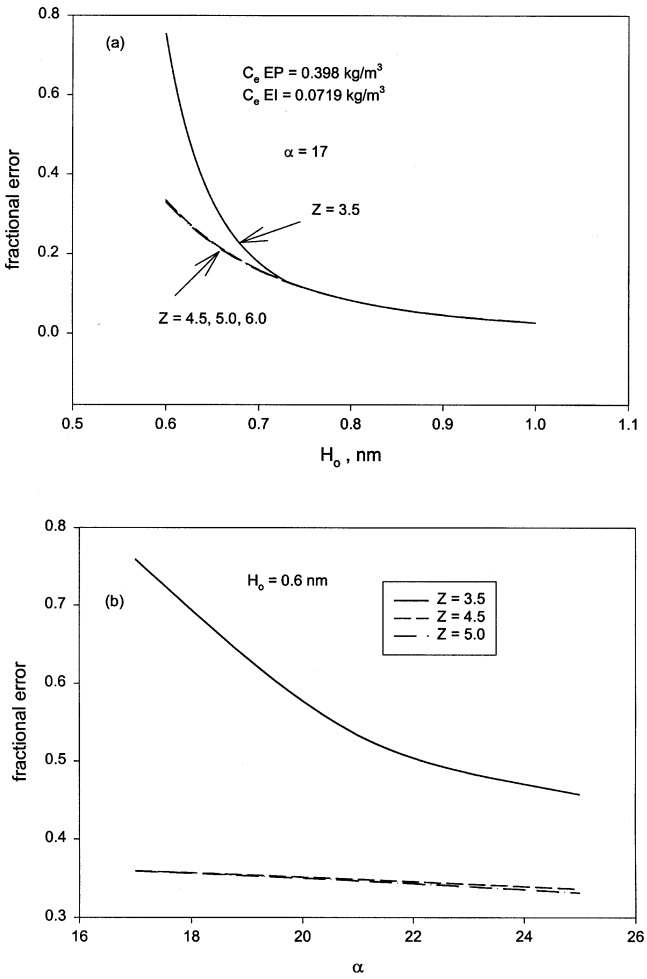

Figure 13. Effect of gamma-function parameter on the fraction of error in ethyl propionate adsorbed at various mean coordination number, if percolation effects are neglected.

Effect of (a) mean pore width and (b) parameter α.

with mean pore width

$$H_o = \frac{\alpha + 1}{w} \tag{35}$$

where α and w are pore structural parameters. In random pore networks, the pore network connectivity, quantified as a mean coordination number, has an important effect on the adsorption of large molecules in small micropores. For the carbons with small mean pore widths, the available pores are accessible to the probe molecules only at sufficiently high mean coordination numbers. The accessibility of the pores decreases with the decrease in the mean coordination number, and below a minimum coordination number, $Z_{\min}$, all the pores are completely inaccessible. Figure 10 shows the effect of mean pore width, H_o, on the minimum coordination number and the selectivity at $\alpha = 20.21$. The minimum value of coordination number Z decreases with the increase in the mean pore width, H_o, as indicated in Figure 10a. Figure 10b depicts the variation in the selectivity of ethyl isovalerate relative to ethyl propionate, with mean pore width H_o at different coordination number, Z. The selectivity of ethyl isovalerate relative to ethyl propionate, $S_{EI,EP}$, follows

$$S_{EI,EP} = \frac{x_{EI}/y_{EI}}{x_{EP}/y_{EP}} \tag{36}$$

where x_{EI} and x_{EP} are the mole fractions of ethyl isovalerate and ethyl propionate in the adsorbed phase, respectively, while y_{EI} and y_{EP} are the mole fractions of ethyl isovalerate and ethyl propionate in the bulk liquid phase, respectively. It is clearly seen that the selectivity of ethyl isovalerate relative to ethyl propionate increases with the mean pore width, H_o. At a mean pore width greater than about 1.0 nm, the variation of the mean coordination number, Z, does not have a significant effect on the selectivity. It is also seen that at a small mean pore width (0.5 nm $< H_o <$ 0.6 nm), the selectivity increases with the increase in the mean coordination number value.

The effect of pore structural parameter α on the minimum coordination number and selectivity of ethyl isovalerate relative to ethyl propionate for $H_o = 0.6$ nm is presented in Figure 11. The parameter α has an inverse relationship with the spread of the PSD at fixed H_o; it is readily seen from Eq. 33 that the variance of the PSD is given by

$$\sigma_v^2 = \int_0^\infty (H - H_0)^2 f_n \, dH = \frac{H_o^2}{(\alpha + 1)} \tag{37}$$

From Figure 11 it can be seen that the minimum coordination number and selectivity of ethyl isovalerate relative to ethyl propionate increase with the increase in the spread of the distribution. From Figures 10 and 11 it is clear that the mean coordination number and selectivity are strongly effected by the mean pore width, and activated carbon with a high mean pore width is more effective for the removal of compounds with a bigger critical molecular size.

The effects of the pore structural parameter on the fraction of error on the amount of ethyl propionate adsorbed, if the percolation effect is neglected, are shown in Figures 12 and 13. The fractional error is defined as

$$\text{Error} = \left| \frac{q_{\text{cal}} - q_{\text{app}}}{q_{\text{app}}} \right| \tag{37}$$

where q_{cal} is the amount adsorbed calculated from the model incorporating percolation effect, and q_{app} is the amount adsorbed calculated from Eq. 33, with the pure-component isotherm following Eq. 20. Figure 12 shows the effect of the pore structural parameter on fractional error in the amount of ethyl propionate adsorbed at $Z = 3.5$. From this figure it can be seen that percolation effects are significant at pore widths smaller than about 0.75 nm, and are less important with an increase in the mean pore width. Figures 13a and 13b depict the effect of coordination number Z on fractional error in the amount of ethyl propionate adsorbed, as a function of the mean pore width and of parameter α, respectively. As expected, the fractional error decreases with the increase in the mean pore width. At a large pore width (> 0.75 nm), the percolation effect is less important, since the compounds can easily penetrate the pores and all available pores are accessible to the compounds.

Conclusions

The connectivity of the pore network is an important aspect of the structure of porous materials, since it influences their reaction and transport properties. The effect of the pore-network connectivity on the prediction of binary component adsorption equilibria is studied. The ideal adsorbed solution theory (IAST) is used in conjunction with the modified DR single-component isotherm, and it is found that incorporation of the connectivity can improve the performance of the multicomponent isotherm model in predicting experimental binary adsorption equilibria.

Literature Cited

Appel, W. S., M. D. LeVan, and J. E. Finn, "Nonideal Adsorption Equilibria Described by Pure Component Isotherms and Virial Mixture Coefficients," *Ind. Eng. Chem. Res.*, **37**, 4774 (1998).

Chen, Y. D., J. A. Ritter, and R. T. Yang, "Nonideal Adsorption from Multicomponent Gas Mixtures at Elevated Pressure on 5A Molecular Sieves," *Chem. Eng. Sci.*, **45**, 2877 (1990).

Costa, E., J. L. Sotelo, G. Calleja, and C. Marron, "Adsorption of Binary and Ternary Hydrocarbon Mixtures on Activated Carbon," *AIChE J.*, **27**, 5 (1981).

Dunne, J., and A. L. Myers, "Adsorption of Gas Mixtures in Micropores: Effect of Difference in Size of Adsorbate Molecules," *Chem. Eng. Sci.*, **49**, 2941 (1994).

Gusev, V., J. A. O'Brien, C. R. C. Jensen, and N. A. Seaton, "Theory for Multicomponent Adsorption Equilibrium: Multispace Adsorption Model," *AIChE J.*, **42**, 2773 (1996).

Hu, X., and D. D. Do, "Comparing Various Multicomponent Adsorption Equilibrium Models," *AIChE J.*, **41**, 1585 (1995).

Ismadji, S., and S. K. Bhatia, "Investigation of Network Connectivity in Activated Carbons by Liquid Phase Adsorption," *Langmuir*, **16**, 9303 (2000).

Ismadji, S., and S. K. Bhatia, "The Use of Liquid Phase Adsorption Isotherms for Characterization of Activated Carbons," *J. Colloid Interface Sci.*, 244, 319 (2001a).

Ismadji, S., and S. K. Bhatia, "A Modified Pore-Filling Isotherm for Liquid-Phase Adsorption in Activated Carbon," *Langmuir*, **17**, 1488 (2001b).

Ismadji, S., and S. K. Bhatia, "Characterization of Activated Carbons Using Liquid Phase Adsorption," *Carbon*, **39**, 1237 (2001c).

Jensen, C. R. C., N. A. Seaton, V. Gusev, and J. A. O'Brien, "Prediction of Multicomponent Adsorption Equilibrium Using a New Model of Adsorbed Phase Nonuniformity," *Langmuir*, **13**, 1205 (1997).

Jossens, L., J. M. Prausnitz, W. Fritz, E. U. Schlunder, and A. L. Myers, "Thermodynamics of Multi-Solute Adsorption from Dilute Aqueous Solutions," *Chem. Eng. Sci.*, **33**, 1097 (1978).

Lavancy, A., M. Stoeckli, C. Wirz, and F. Stoeckli, "Binary Adsorption of Vapours in Active Carbons Described by the Dubinin Equation," *Adsorption Sci. and Technol.*, **13**, 537 (1996).

Lee, C. K., and C. S. Tsay, "Pore Connectivity of Alumina and Aluminium Borate from Nitrogen Isotherms," *J. Chem. Soc., Faraday Trans.*, **94**, 573 (1998).

Lopez-Ramon, M. V., J. Jagiello, T. J. Bandosz, and N. A. Seaton, "Determination of the Pore Size Distribution and Network Connectivity in Microporous Solids by Adsorption Measurements and Monte Carlo Simulation," *Langmuir*, **13**, 4435 (1997).

Moon, H., and C. Tien, "Adsorption of Gas Mixtures on Adsorbents with Heterogeneous Surfaces," *Chem. Eng. Sci.*, **43**, 2967 (1988).

Murray, K. L., N. A. Seaton, and M. A. Day, "Analysis of the Spatial Variation of the Pore Network Coordination Number of Porous Solids Using Nitrogen Sorption Measurements," *Langmuir*, **14**, 4953 (1998).

Murray, K. L., N. A. Seaton, and M. A. Day, "Use of Mercury Intrusion Data, Combined with Nitrogen Adsorption Measurements, as a Probe of Pore Network Connectivity," *Langmuir*, **15**, 8155 (1999).

Myers, A. L., and J. M. Prausnitz, "Thermodynamics of Mixed Gas Adsorption," *AIChE J.*, **11**, 121 (1965).

Neimark, A. V., "Percolation Theory of Capillary Hysteresis Phenomena and its Application for Characterization of Porous Solids," *Characterization of Porous Solids II*, F. Rodriguez-Reinoso, J. Rouquerol, K. S. W. Sing, and K. K. Unger, eds., Elsevier, Amsterdam (1991).

Radke, C. J., and J. M. Prausnitz, "Thermodynamics of Multi-Solute Adsorption from Dilute Liquid Solutions," *AIChE J.*, **18**, 761 (1972).

Richter, E., W. Schutz, and A. L. Myers, "Effect of Adsorption Equation on Prediction of Multicomponent Adsorption Equilibria by Ideal Adsorbed Solution Theory," *Chem. Eng. Sci.*, **44**, 1609 (1989).

Sahimi, M., *Applications of Percolation Theory*, Taylor & Francis, London (1994).

Sandler, S. I., *Chemical and Engineering Thermodynamics*, Wiley, New York (1999).

Seaton, N. A., "Determination of the Connectivity of Porous Solids from Nitrogen Sorption Measurements," *Chem. Eng. Sci.*, **46**, 1895 (1991).

Steele, W. A., "Physical Interaction of Gases with Crystalline Solids: I. Gas-Solid Energies and Properties of Isolated Adsorbed Atoms," *Surf. Sci.*, **36**, 317 (1973).

Suwanayuen, S., and R. P. Danner, "A Gas Adsorption Isotherm Equation Based on Vacancy Solution Theory," *AIChE J.*, **26**, 68 (1980).
Talu, O., and I. Zwiebel, "Multicomponent Adsorption Equilibria of Nonideal Mixtures," *AIChE J.*, **32**, 1263 (1986).
Valenzuela, D. P., and A. L. Myers, "Gas Adsorption Equilibria," *Sep. Purif. Methods*, **13**, 152 (1984).
Valenzuela, D. P., A. L. Myers, O. Talu, and I. Zwiebel, "Adsorption of Gas Mixtures: Effect of Energetic Heterogeneity," *AIChE J.*, **34**, 397 (1988).
Valenzuela, D. P., and A. L. Myers, *Adsorption Equilibrium Data Handbook*, Prentice Hall, Englewood Cliffs, NJ (1989).
Yang, R. T., *Gas Separation by Adsorption Processes*, Butterworth, New York (1987).
Yun, J. H., H. C. Park, and H. Moon, "Multicomponent Adsorption Calculations Based on Adsorbed Solution Theory," *Korean J. Chem. Eng.*, **13**, 246 (1996).
Zhang, L., and N. A. Seaton, "Simulation of Catalyst Fouling at the Particle and Reactor Levels," *Chem. Eng. Sci.*, **51**, 3257 (1996).
Manuscript received Oct. 8, 2001, and revision received June 17, 2002.